TECHNICAL NOTE

Series Ni–Ti shape memory alloy wires with different martensitic–austenitic phase transformation temperatures as an actuator for input shaping control

IOP Publishing Smart Materials and Structures
Smart Mater. Struct. **28** (2019) 077001 (13pp) https://doi.org/10.1088/1361-665X/ab1941

Technical Note

Series Ni–Ti shape memory alloy wires with different martensitic–austenitic phase transformation temperatures as an actuator for input shaping control

Gwang-Yong Jung, Seung-Bok Choi and Gi-Woo Kim

Department of Mechanical Eng., Inha University, Incheon, Republic of Korea

E-mail: gwkim@inha.ac.kr

Received 15 December 2018, revised 28 February 2019
Accepted for publication 15 April 2019
Published 21 May 2019

Abstract

This study presents series shape memory alloy (SMA) wire actuators featuring different martensitic–austenitic phase transformation temperatures for input shaping control of flexible structures, such as compliant robot manipulators. Similar to conventional electric motors, the proposed actuator can generate stair-wise input shaping commands by simply applying a step current input. A practical input shaping control of flexible structures (e.g. beam manipulator) actuated by a series SMA wire actuator with different martensitic–austenitic phase transformation temperatures was proposed, and its ability to suppress residual vibration was successfully validated through simulation and laboratory experiments.

Supplementary material for this article is available online

Keywords: shape memory alloy, phase transformation temperature, series SMA wire actuator, input shaping control, residual vibration, flexible structures

(Some figures may appear in colour only in the online journal)

1. Introduction

Flexible structures, such as large deployable structures and robot manipulators, need to be lightweight for high power efficiency (or density). Moreover, space structures should particularly be designed in the form of lightweight deployable structures considering the need for efficient space utilization and cost-effective launching [1]. Since 1980, a few solar sail systems (e.g. HELIOS, IKAROS) and gossamer deorbiter systems have been developed and studied using the rollable blade, Miura folding, and bistable boom for the flexible and deployable large space structures [2–6]. However, light and flexible structures with low damping ratios can be deformed, causing residual vibrations owing to the low energy dissipation during position control [7]. Such unwanted residual vibrations may lead to inaccurate position control performance; hence, there have been much research efforts on flexible structure control have been attempted [8–11].

Input shaping, or command shaping, control has been known to be an effective control method to suppress the residual vibrations induced by the position control response of light-damped systems [12]. Studies such as those by Song *et al* [13] and Hu *et al* [14] have reported the application of input shaping control to flexible space structures. This control strategy, namely the open loop control system, is easy to implement because it does not require measuring sensors. In the late 1950s, systematic command shaping was studied by Smith [15]. However, the conventional actuators used for input shaping control, such as electric motors, are typically not suitable for vibration control of lightweight flexible

structures in space because of the low power density and complicated actuator structure including drivers and electric circuitry [1].

To overcome these technical limitations, significant research efforts on the vibration control of flexible structures have been attempted over the last decades through the use of smart materials-based actuators such as piezoelectric materials, magnetorheological (MR) fluids, and shape memory alloys (SMAs). For example, vibration control of a cantilever beam by employing a piezoelectric polymer actuator attached to a cantilever beam was studied by Bailey *et al* [16]. Similarly, Han *et al* [17] studied the optimum positions of piezoelectric sensors and actuators a using genetic algorithm (GA) for the vibration control of a composite plate. Choi *et al* studied the vibration reduction of a flexible beam structure due to external disturbances using a mixed-mode MR mount with a linear quadratic Gaussian controller [18]. Lara-Prieto *et al* also investigated the reduction of residual vibration by applying a magnetic field to the MR cantilever sandwich beam with the MR fluid inserted in two elastic layers to change the stiffness of the beam structures [19]. Nevertheless, SMA-based actuators are attractive alternative actuation systems because of their high power density and simple structure. Furthermore, the strain (or stroke) of the SMA wires during the contraction phase is larger than that of the other smart materials such as piezoelectric transducers, typically about 4%–5% of their initial length [20]. SMA actuators for flexible structure control applications can be categorized using various actuation configurations in terms of their loading types. However, most SMA-based actuator designs are based on a single SMA spring-wire type because they can generate a large stroke change with relatively small microscopic strain, and their fabrication process is simple—annealing an SMA wire wound on a rod [21]. Baz *et al* studied the vibration reduction of the flexible beam using two SMA wires mounted on both sides of the beam as actuators [22]. Sohn *et al* studied two SMA wires symmetrically mounted on the neutral axis of the beam with a sliding mode controller to control the residual vibration. This study demonstrates a robust residual vibration reduction performance against the uncertainty of response time during the heating and cooling of the SMA wire [23]. To date, no previous study has been attempted on the development of series Ni–Ti SMA wire with different martensitic–austenitic phase transformation temperatures as one of alternative actuators for input shaping control of a flexible structure, although various versions of SMA wire actuators can be found in prior art or recent literatures related to the SMA technology [24–33].

Therefore, the objective of this study is to design a new type of SMA wire actuator for input shaping control of flexible structures by simply connecting two SMA wires with different phase transformation temperatures in series, aimed at producing stair-wise input shaping command that is similar to the input shaping command achieved by the conventional electric motor actuators. The proposed series SMA wire actuator is simple but effective for suppressing residual vibration because it can produce a stair-wise input shaping command despite the application of a step input, whereas it is necessary to control an electric motor using an electric driver and a complicated motor controller such as pulse width modulation. Section 2 describes the new actuation concept using the proposed SMA wire actuator. Section 3 describes the dynamic modeling of the flexible beam manipulator with the SMA wire actuator. In section 4, the SMA wire actuator is applied to input shaping control, and the optimum phase transformation temperature for the suppression of residual vibration is simulated using optimization algorithms, such as the GA. Finally, a preliminary experimental study on the SMA wire actuator is presented, and its fundamental performance is successfully evaluated for the first time.

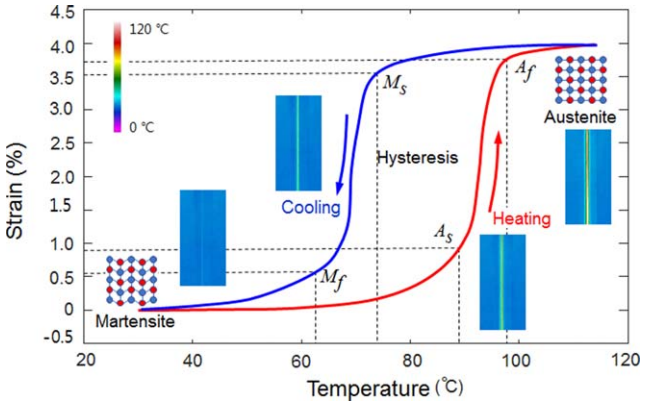

Figure 1. Typical phase transformation curve of a single SMA wire (FLEXINOL® Actuator Wires, $\phi = 150\ \mu$m, HT). Insert: thermographic images.

2. Design of a series SMA wire actuator

SMAs are a class of metals that undergo phase transformation, known as the shape memory effect, when exposed to magnetic fields or temperature gradients: when the temperature is increased via Joule heating beyond the threshold temperature, the, SMAs undergo phase transformation from martensite to austenite, leading to contraction and thereby deformation. Conversely, during the cooling process, a phase change occurs in the SMAs from austenite to martensite, which restores their original shape [21]. While the temperature increase is electrically controlled through internal Joule heating, the cooling is simply controlled by the process of convection in the surrounding air. The SMAs can exist in two different phases that can have three different crystal structures: twinned martensite, detwinned martensite, and austenite. The austenite phase is stable at high temperatures; whereas, the martensite phase is stable at lower temperatures. Figure 1 represents a typical phase transformation curve and the thermographic image captured by an infrared thermal image camera (FLIR, T650sc; minimum spot size: 100 μm) of a commercial SMA wire (ϕ =150 μm) [34]. Upon heating the SMA, as shown in the thermographic image in figure 1, the initial martensite phase begins to transform into the austenite phase: A_s is the onset temperature at which, the austenite transformation begins, and A_f is the terminal temperature at

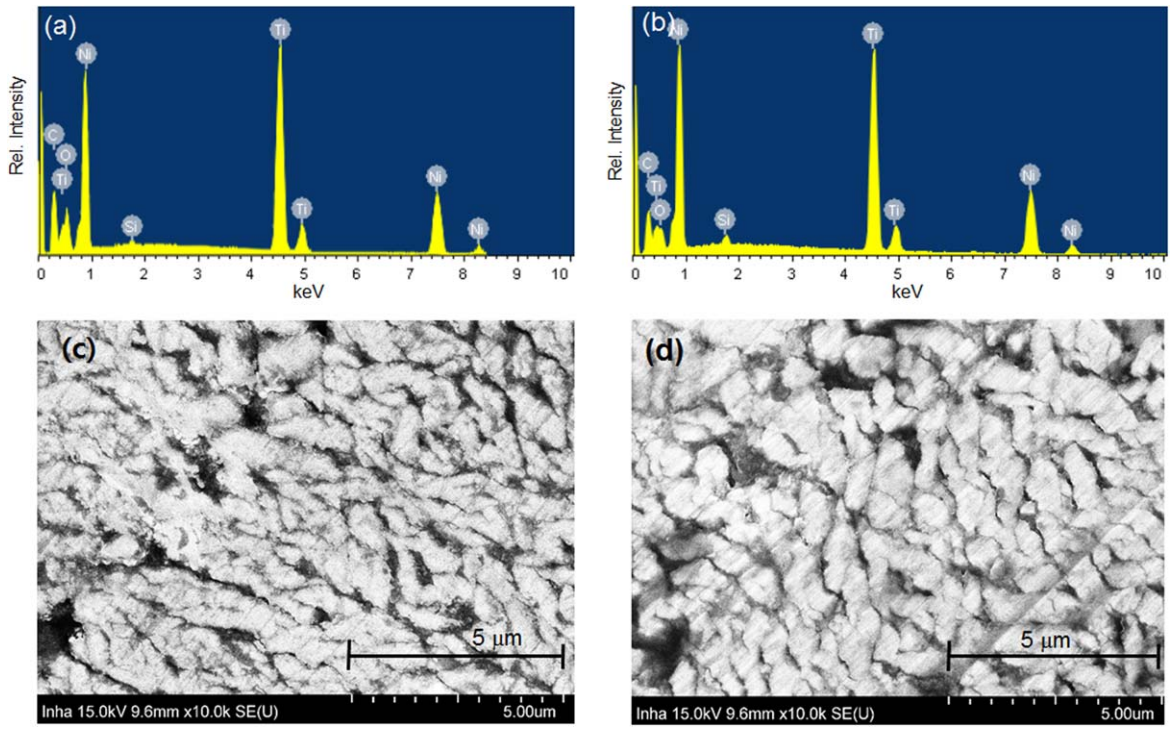

Figure 2. EDS spectra and microscopic SEM images (×10k) the two SMA wires: (a) EDS of LT SMA wire, (b) EDS of HT SMA wire, (c) SEM image of LT SMA wire, and (d) SEM image of HT SMA wire.

which, the transformation is complete. Once the SMA is heated beyond A_s, it begins to transform into austenite, which cause contraction and deformation. On cooling, the transformation is reversed, i.e. from austenite to martensite at the onset temperature M_s, at which the martensite transformation begins, and is complete when it reaches the terminal temperature M_f. In this study, two SMA wires with different martensitic–austenitic phase transformation temperatures (i.e. A_s), low temperature (LT; 154.4°F (68 °C)) and high temperature (HT; 190.4°F (88 °C)), are used for series SMA actuator.

The surface morphology of the two SMA wires was observed using a scanning electron microscope (SEM), and an energy-dispersive x-ray spectroscopy (EDS) analyzer (Horiba EX-250) was used to identify the chemical characterization of the two SMA wires in which the nickel and titanium components are uniformly dispersed throughout the matrix. Figures 2(a) and (b) show the results of EDS of LT and HT SMA wire, respectively. Typically, it enable to us to change the critical transition temperature either by a slight change in the Ti/Ni composition or by replacing the cobalt component in the alloy with nickel [35]. In this study, the start temperature of austenite (A_s) of the SMA wire can be changed from 154.4°F to 190.4°F by increasing the weight of nickel component. (38.83% [$Ni_{39}Ti_{33}$] → 43.98% [$Ni_{44}Ti_{37}$].)

The proposed SMA wire actuator features two SMA wires connected in series with different phase transformation temperatures (HT and LT), as shown in figure 3(a). The operation principle of the proposed actuator is as follows: when the input current is applied to the SMA wire actuator, the temperature increases owing to internal Joule heating.

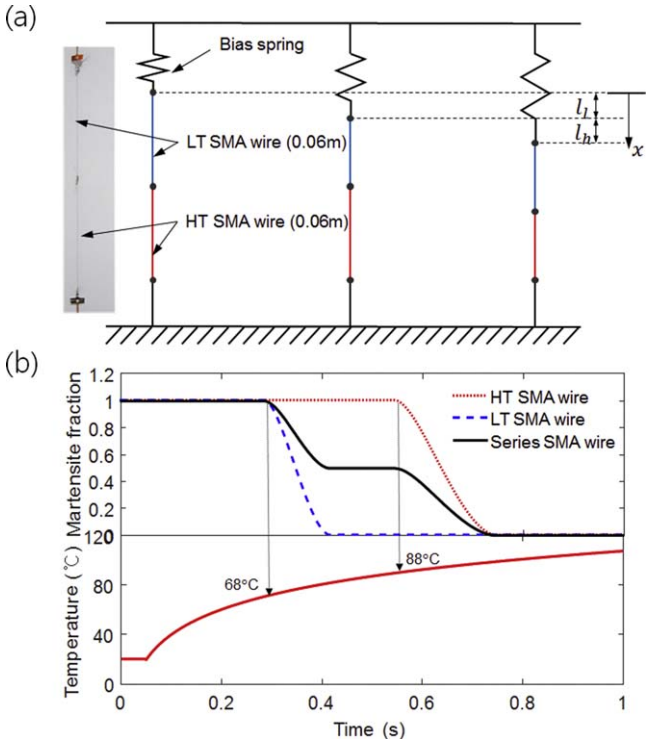

Figure 3. Schematic of the proposed series SMA wire actuator: (a) actuating concept and photograph, (b) martensite volume fraction curve of SMA wires and their temperature increase.

Because the SMA wire is short and thin (0.12 m, $\phi = 150\ \mu$m), the resistance change between the martensite and the austenite phases is not significant. Therefore, the temperature distribution in the series SMA wire during the

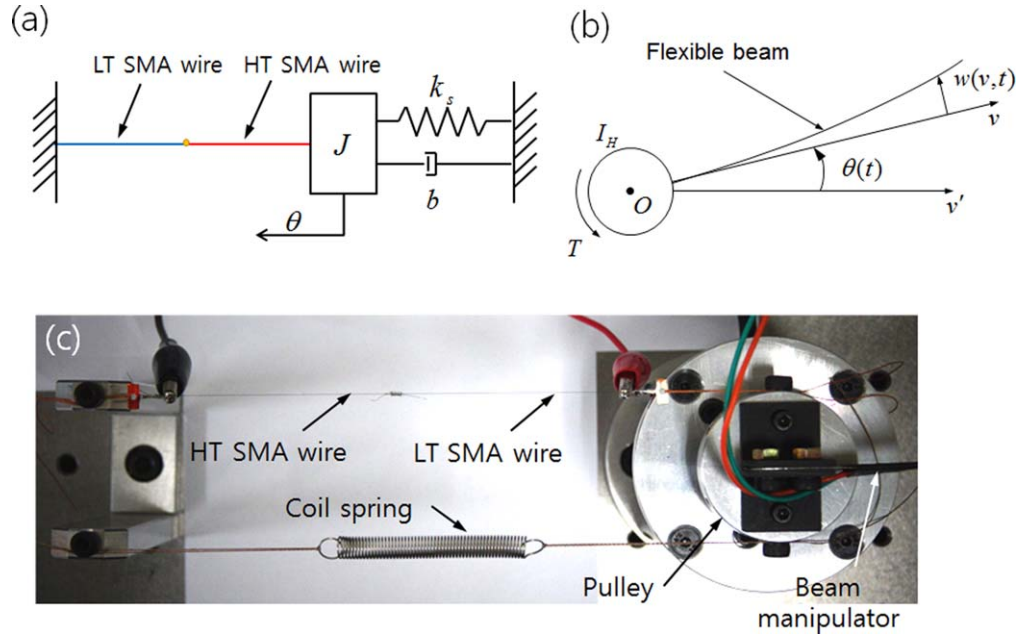

Figure 4. Schematic of a flexible beam manipulator combined with a series SMA wire actuator: (a) equivalent mechanical model, (b) single-link flexible manipulator model, and (c) overall photograph.

heating is uniform, as shown in figure 3(b). We experimentally observe that as the temperature increases, the LT SMA wire first reaches the phase transformation temperature, and transforms from martensite into austenite and therefore, shrinks. The HT SMA wire subsequently transforms when the temperature continues to increase and reaches its transformation temperature; l_l and l_h represent the contraction lengths of the LT and HT SMA wires, respectively. Because the diameter of the series SMA wire is constant, the stress applied to the LT and HT SMA wires also the same. In addition, the chemical composition of the two SMA wires is uniformly distributed as seen in the SEM image (see figure 2). Therefore, it can be assumed that the martensite fraction of the series SMA wire at a specific time is significantly related to the ratio of the length of the LT and the HT SMA wires.

By assuming that the volume fraction of the martensite is proportional to the length ratio of the SMA wires, it is reasonable that the total martensite fraction can be determined by the weighted average of the two martensite fractions in the two SMA wires. This is because the martensite fraction in the SMA wire is a measure of the extent of phase transformation, which is expressed as follows:

$$\xi = \alpha\xi_1 + (1 - \alpha)\xi_2, \tag{1}$$

where ξ_1, ξ_2, and ξ are the martensite fractions of the HT SMA wire, LT SMA wire, and series SMA wire, respectively; and α is the length ratio of the HT SMA wire to the series SMA wire (its value ranges from 0 to 1). For example, when both HT and LT SMA wires are completely transformed, we have: $\xi_1 = \xi_2 = 0$ and therefore, $\xi = 0$, as shown in figure 3(b). Therefore, the proposed SMA wire actuator possesses a two-step linear motion through this process, which in turn produces a stair-wise input shaping control action. The amplitude ratio of each signal can be adjusted by controlling the ratio of the lengths of the HT and LT SMA wires, while the time location can be controlled by the difference between the phase transformation temperatures of the HT and LT SMA wires. Furthermore, a bias coil spring is also installed at one end of the series SMA wire actuator; and the two SMA wires with different phase transformation temperatures are connected using a crimp bead. The actuation force generated due to contraction causes the pulley to rotate, and the resulting torque determines the position of the flexible structure. Figure 4(a) shows the equivalent mechanical model, and figure 4(b) shows the flexible beam manipulator model.

3. Modeling of series SMA wire actuator and flexible beam manipulator

3.1. Heat transfer model of the SMA wire

The input current increases the temperature of the SMA wire via Joule heating. Then, the balance of heat energy governs the temperature of the SMA wire. The following heat transfer model is formulated to describe the rate of temperature change $\dot{T}$ due to a change in the current I in the wire and the convective heat lost to the environment:

$$m_w l_0 c_p \dot{T} = I^2 R l_0 - hA_w(T - T_{amb}), \tag{2}$$

where m_w is the mass per unit length, l_0 is the initial length of the specimen, c_p is the specific heat capacity, R is the resistance per unit length, A_w is the surface area of the specimen, T_{amb} is the ambient temperature, and h is the heat convection factor with parameters h_0 and h_2 ($h = h_0 + h_2 T^2$) [27].

3.2. Phase transformation model of the SMA wire

During the heating and cooling processes, the martensite fraction of the SMA wire is determined by the temperature and stress applied to it [36]. The martensite fraction during phase transformation from martensite to austenite during heating (for $A_s + \sigma/C_A \leqslant T \leqslant A_f + \sigma/C_A$) may be defined as follows:

$$\xi = \frac{\xi_M}{2}\{\cos[a_A(T - A_s) + b_A\sigma] + 1\}. \tag{3}$$

Conversely, during cooling (for $M_f + \sigma/C_M \leqslant T \leqslant M_s + \sigma/C_M$), the phase of the SMA wire transforms from austenite to martensite, and the martensite fraction is defined as follows:

$$\xi = \frac{1 - \xi_A}{2}\cos[a_M(T - M_f) + b_M\sigma] + \frac{1 + \xi_A}{2}, \tag{4}$$

where σ is the stress; ξ_M and ξ_A are the initial martensite fractions of each phase transformation; and C_A and C_M are the stress influence coefficient at austenite and martensite phase, respectively. The constants a_A, b_A, a_M, and b_M can be derived as follows using the four transformation temperatures: $a_A = \pi/(A_f - A_s)$, $b_A = -(a_A/C_A)$ and $a_M = \pi/(M_s - M_f)$, $b_M = -(a_M/C_M)$.

3.3. SMA wire actuator model

The Liang constitutive model was used to derive the induced normal stress associated with the nonlinear stiffness of the SMA wire [36]. The stress change rate ($\dot{\sigma}$) is a function of the rate of strain ($\dot{\varepsilon}$), temperature change rate ($\dot{T}$), and martensite fraction change rate ($\dot{\xi}$) in the SMA wire and is calculated as follows:

$$\dot{\sigma} = E\dot{\varepsilon} + \Omega\dot{\xi} + \Theta\dot{T}, \tag{5}$$

where E is the Young's modulus and is represented by: $E = \xi E_M + (1 - \xi)E_A$; E_M and E_A are the Young's moduli corresponding to martensite and austenite phases of the SMA, respectively; and Ω and Θ are the phase transformation constant and thermal coefficient of expansion, respectively. The phase transformation constant can be expressed as follows:

$$\Omega = -\varepsilon_L E, \tag{6}$$

where ε_L is the maximum residual strain, while the thermal coefficient of expansion is negligible. Therefore, equation (5) is simplified as follows:

$$\dot{\sigma} = E\dot{\varepsilon} - \varepsilon_L E\dot{\xi}. \tag{7}$$

The strain rate of SMA wire ($\dot{\varepsilon}$) in equation (7) is derived from kinematics as a function of its joint velocity $\dot{\theta}$ as follows:

$$\dot{\varepsilon} = -r\left(\frac{\dot{\theta}}{l}\right), \tag{8}$$

where r and l are the radius of the pulley and length of the SMA wire, respectively. Thus, the actuation force F can be calculated by multiplying the cross-sectional area of the SMA wire A and the stress σ after integrating the stress change rate (i.e. $F(t) = A\sigma$). The dynamics of the series SMA wire actuators is then developed on the basis of the mechanical model, as shown in figure 4(a). The equation of motion for the series SMA actuator is written as follows:

$$J\ddot{\theta} = \sum T(t) = [F(t) - b\dot{\theta} - k_s\theta]r, \tag{9}$$

where J, b, and k_s are the moment of inertia, damping coefficient, and stiffness of the coil spring, respectively.

3.4. Flexible beam manipulator model

As shown in figure 4(b), the rotation angle of the pulley from the fixed axes ov' is θ, the length from the pulley to the flexible beam is v, and the deformation of the flexible beam from the neutral axis v is w. Therefore, the total displacement u of the beam manipulator can be expressed as follows:

$$u(v, t) = w(v, t) + v\theta(t). \tag{10}$$

The total displacement in equation (10) can be expressed as follows using the assumed mode method [37]:

$$u(v, t) = \sum_{i=0}^{\infty} \Phi_i(v)q_i(t), \tag{11}$$

where the length function $\Phi_i(v)$ and time function $q_i(t)$ are the eigenfunctions of the ith mode and the generalized coordinates of the system, respectively. By applying the Lagrange's equation, a decoupled ordinary differential equation for each vibration mode is formulated as follows:

$$(\ddot{q}_i + 2\varsigma_i\omega_i\dot{q}_i + {\omega_i}^2 q_i) = \frac{1}{J}\Phi'(0)T(t), \tag{12}$$

where $T(t)$ is the torque input induced by the stress (σ) of the SMA wire; and ς_i and ω_i are the damping ratio and natural frequency of the ith mode, respectively.

In this study, only the first mode has been considered because excitation of the higher vibration modes is not likely. MATLAB/Simulink® provided by MathWorks™ was used to numerically solve a system of integral equations [38]: the 4th order Runge–Kutta method (ode4) with a fixed-step size of 0.001 s was selected for the stable numerical integration. The block diagram and overall Simulink model for the simulation and optimization are shown in figure 5. The block diagram includes the LT and HT SMA submodel, consisting of the heat transfer model, phase transfer model, constitutive model, dynamics, and kinematics.

4. Application to input shaping control

4.1. Overview of input shaping control

Input shaping control is an effective open-loop control scheme that suppresses residual vibration generated during position control of the flexible system. The concept of this open-loop control is to divide the reference input into two signal sequences using the natural frequency and damping ratio of the system, and then to cancel the oscillation induced by the first signal with the second signal, as shown in figure 6.

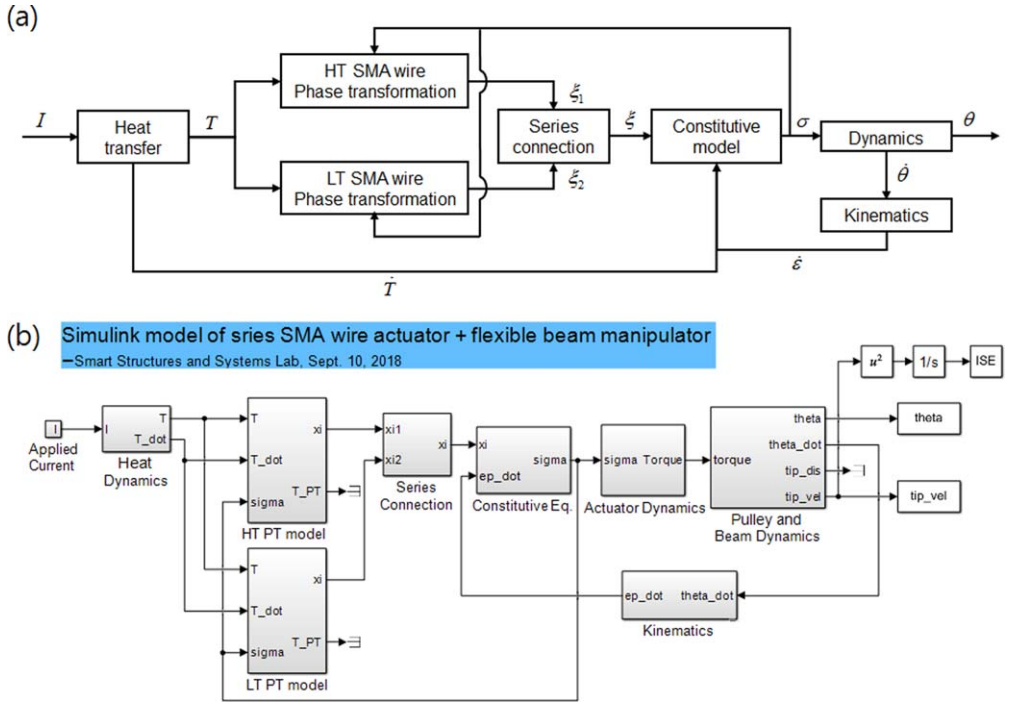

Figure 5. Simulation model of a series SMA wire actuator combined with a flexible beam manipulator: (a) block diagram of the SMA wire actuator, (b) overall MATLAB/Simulink model.

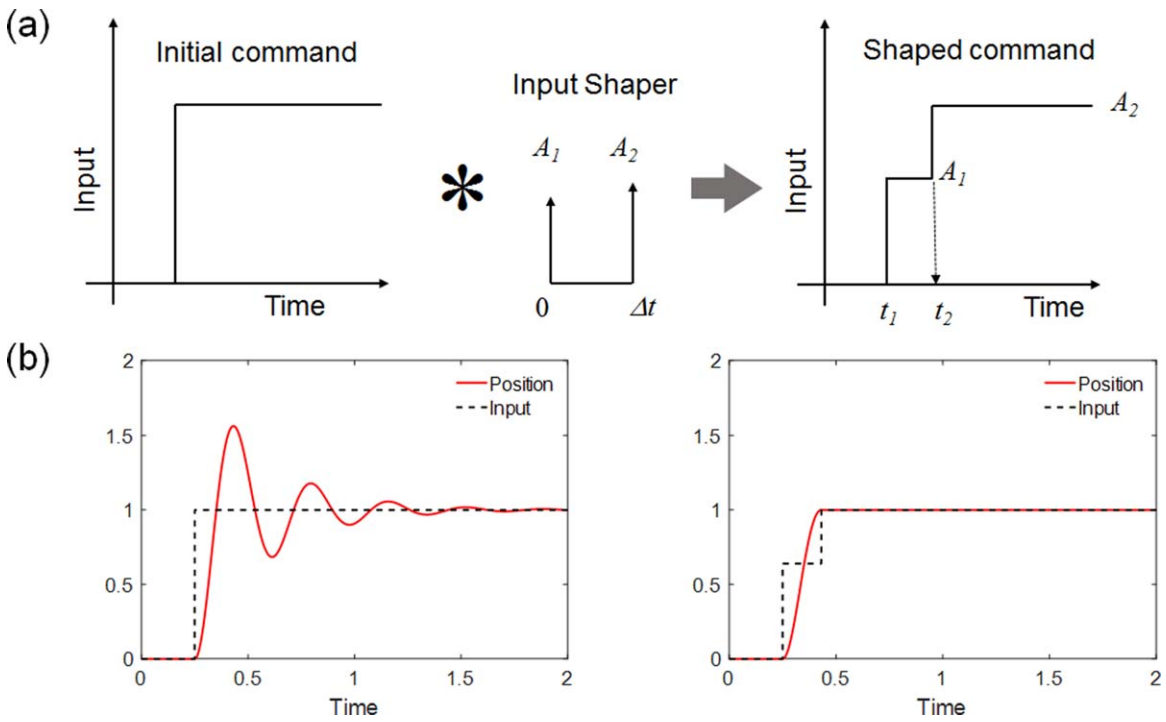

Figure 6. Schematic of input shaping control (ZV shaper): (a) convolution product of initial command and input shaper, and stair-wise shaped command, and (b) response of each command.

The residual vibration (V) generated by each signal can be expressed as follows, using the natural frequency (ω_n) and damping ratio (ς) [12]

$$V(\omega, \varsigma) = \exp(-\varsigma\omega t_n)\sqrt{C(\omega, \varsigma)^2 + S(\omega, \varsigma)^2}, \qquad (13)$$

where $C(\omega, \varsigma)$ and $S(\omega, \varsigma)$ are defined as follows:

$$C(\omega, \varsigma) = \sum_{i=1}^{n} A_i e^{\varsigma\omega t_i} \cos(\omega_d t_i); \; S(\omega, \varsigma) = \sum_{i=1}^{n} A_i e^{\varsigma\omega t_i} \sin(\omega_d t_i), \tag{14}$$

where A_i and t_i are the amplitudes and time locations of the sequence, and ω_d is the damped natural frequency expressed as $\omega_d = \omega_n\sqrt{1-\varsigma^2}$. Equation (13) must be equal to zero because the residual vibration should be eliminated. By setting constraints such that the sum of the impulse equals to one (i.e.$\sum A_i = 1$) and the magnitudes of the impulses are finite and positive (i.e. $A_i > 0$) to obtain a nontrivial and bounded solution, a zero vibration (ZV) shaper ($n = 2$) can be obtained as follows [12]:

$$\begin{bmatrix} t_i & A_i \end{bmatrix} = \begin{bmatrix} 0 & \frac{1}{1+K} \\ 0.5T_d & \frac{K}{1+K} \end{bmatrix}, \tag{15}$$

where T_d and K are defined as follows:

$$T_d = \frac{2\pi}{\omega_d}, \; K = \exp\left(\frac{-\varsigma\pi}{\sqrt{1-\varsigma^2}}\right). \tag{16}$$

The proposed series SMA wire actuator with two different phase transformation temperatures can exhibit the input shaping effect. As the ratio of the length of the HT SMA wire to that of the series SMA wire (α) increases, the amplitude of the first step (i.e. A_1 in figure 6(a)) decreases, as shown in figure 7(a). On the other hand, the difference in time location between the first and second steps (i.e. $t_1 - t_2$ in figure 6(a)) increases as the transformation temperature difference increases, as shown in figure 7(b).

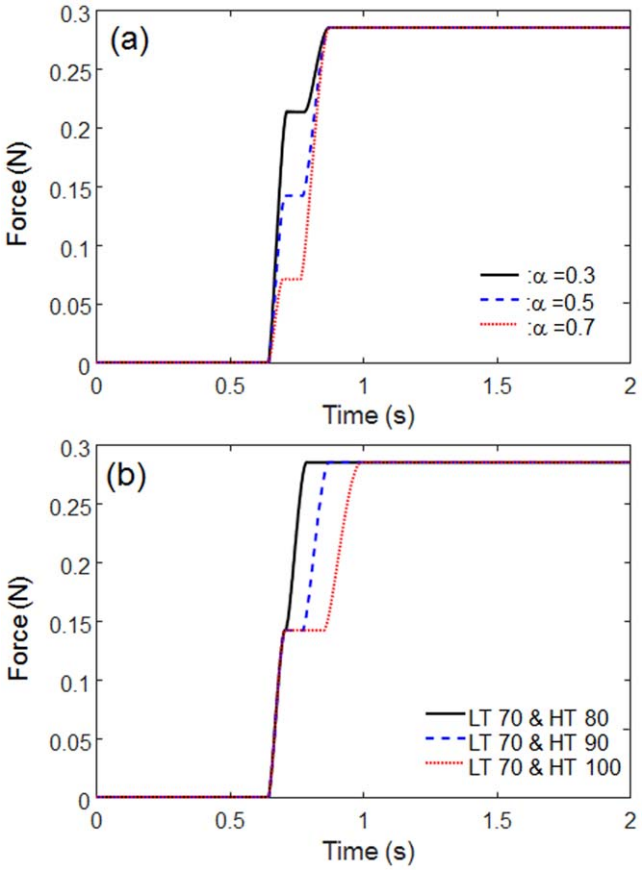

Figure 7. Stair-wise input shaping effect with: (a) varying α, and (b) varying phase transformation of the series SMA wires.

4.2. Optimum phase transformation temperatures

From the operational principle of the new SMA actuator, the rotational angle of the pulley (θ) and the residual vibration of the manipulator beam (V) have the following dependence on the transformation temperatures of the two SMA wires (i.e. HT and LT SMA wires):

$$\theta = f(T_{sL}, T_{sH}), \; V = g(T_{sL}, T_{sH}), \tag{17}$$

where T_{sL} and T_{sH} are the phase transformation temperatures of the LT and HT SMA wires to be regressed. To minimize the residual vibration, the optimum phase transformation temperatures of the HT and LT SMA wires need to be determined. In this study, a GA is employed to determine the optimum phase transformation temperatures by defining two performance indexes (cost or objective functions) calculated from the integration of the square of the error between the motor and pulley rotation angles (i.e. $\theta_m - \theta$) [39]. This optimization problem can also be solved using a different performance index, i.e. the integration of the square of the residual vibration (V). In contrast to the conventional optimization methods, a main advantage of the GA is that it does not require a mathematically well-posed objective function, which is most suitable for the high nonlinearity of the SMA actuation systems. In addition, it is less likely to converge at the local minima or maxima because the GA performs a search in a population of points and is based on probabilistic transition rules. Accordingly, the GA is suitable for solving the following constrained optimization problem [40]:

$$\text{Maximization} - \text{PI}_1 = -\int_0^\infty \{\theta_m(t) - \theta(t)\}^2 dt, \quad -\text{PI}_2 = -\int_0^\infty V(t)^2 dt, \tag{18}$$

Subject to $T_{sL,lower} \leqslant T_{sL} \leqslant T_{sL,upper}$, $T_{sH,lower} \leqslant T_{sH} \leqslant T_{sH,upper}$.

Because the GA can handle only the maximization problem, the performance index is multiplied by -1 and optimized under the bounds: $50 \leqslant T_{sL} \leqslant 70$, $90 \leqslant T_{sH} \leqslant 200$ and the initial population size (20 in this case). On applying the step current input, the best population (i.e. performance index) is converges at the optimum values of -0.001 and -0.1667 after 50 iterations, suggesting two optimum phase transformation temperatures ($T_{sL} = 52.03$ °C, $T_{sH} = 161.15$ °C for PI_1, and $T_{sL} = 64.17$ °C, $T_{sH} = 139.45$ °C for PI_2), as shown in figure 8.

The residual vibration control performance with two optimal phase transformation temperature differences were simulated. All parameters and phase transformation

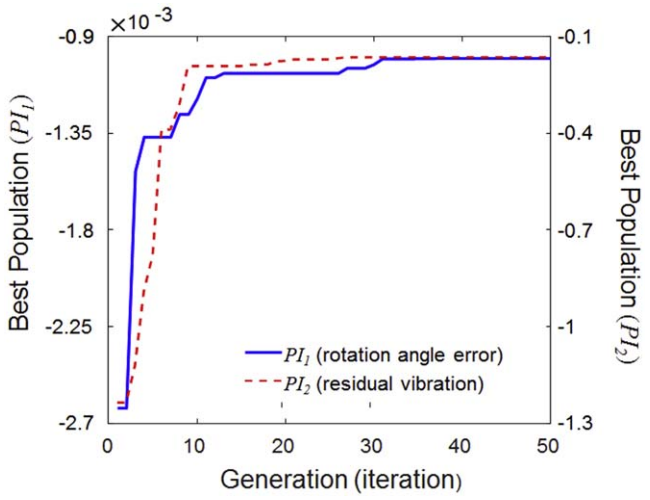

Figure 8. Convergence of the best population according to the performance index. The blue solid line indicates the error between the shaped input and rotation angle of the pulley (converging at −0.001), and the red dotted line indicates the residual vibration (converging at −0.1667).

Table 1. Mechanical and thermal parameters of the SMA wire actuator for simulation.

Parameter (unit)	Description	Value
E_M (GPa)	Young's modulus of martensite phase	28
E_A (GPa)	Young's modulus of austenite phase	75
C_M (MPa K^{-1})	Stress influence coefficient of martensite phase	10
C_A (MPa K^{-1})	Stress influence coefficient of austenite phase	10
R (Ω m^{-1})	Linear resistance of SMA wire	200
m (kg m^{-1})	Mass per unit length of SMA wire	2.85×10^{-5}
l_0 (m)	Initial length of SMA wire	0.12
A (m^2)	Cross-sectional area of SMA wire	4.42×10^{-9}
A_w (m^2)	Surface area of SMA wire	2.83×10^{-5}
ε_L (%)	Maximum residual strain	2.3
c_p (J kg^{-1} °C^{-1})	Specific heat capacity of SMA wire	320
h_0 (W (m^{-2} K^{-1})	Heat convection factor	20
h_2 (W (m^{-2} K^{-3})	Heat convection factor	0.001
T_{amb} (°C)	Ambient temperature	20
J (kg m^2)	Moment of inertia	5.67×10^{-5}
b (kg s^{-1})	Damping coefficient	0.02
k_s (N m^{-1})	Spring constant	40
r (m)	Radius of pulley	0.02

temperatures of the SMA wires are summarized in tables 1 and 2, respectively. In this study, primary mechanical properties (e.g. particularly Young's modulus) of SMA wires at original state (martensite phase) were assumed to be constant based on experimental observation (tensile test) of two commercial SMA wires although it has been known that their mechanical properties can be different if the transformation temperatures are different [35]. As shown in figure 9, the residual vibration can be suppressed using the phase transformation temperature differences optimized by the GA. The time locations (t_i) and amplitudes (A_i) for input shaping control can then be estimated as follows:

$$[t_i\ A_i] = \begin{bmatrix} 0 & 0.5604 \\ 0.1510 & 0.4396 \end{bmatrix} \text{for PI}_1(52\ ^\circ\text{C and } 161\ ^\circ\text{C}),$$
$$[t_i\ A_i] = \begin{bmatrix} 0 & 0.5131 \\ 0.1440 & 0.4869 \end{bmatrix} \text{for PI}_2(64\ ^\circ\text{C and } 139\ ^\circ\text{C}). \quad (19)$$

5. Experimental validation

5.1. Experimental setup

The residual vibration control performance is experimentally evaluated in a simple laboratory-level test-bed, as shown in figure 10. The actuation force time responses and hysteresis curve of the series SMA wire actuator were first measured to present the fundamental actuator characteristics. Next, the performance of the input shaping control using the conventional actuator (BLDC motor) was evaluated and compared with that using the new SMA wire actuator to identify the design parameters (time locations t_i, and amplitudes A_i). Finally, the residual vibration responses of the flexible beam manipulator actuated by an SMA wire actuator were investigated to demonstrate the concept of the new SMA actuator for the input shaping control application proposed in section 2.

A miniature load cell (LSB200, Futek) was used to measure the actuation force. The shrink length (i.e. stroke) of the SMA wire was also measured using a laser vibrometer (IL-300, KEYENCE). In this study, a preliminary input shaping control experiment with a flexible beam manipulator and an electric motor was first conducted to demonstrate the ZV shaper and to design the stair-wise input that will be generated by the SMA wire actuator, which is simply connected by two SMA wires with different phase transformation temperatures. Figure 10(b) shows the experimental setup for implementing a ZV shaper using a BLDC motor (AKM21E, National Instruments) and an embedded real-time control board (NI cRio-9030, National Instruments). The BLDC motor was controlled using the closed-loop proportional-integral (PI) control. The flexible cantilever beam (180 mm × 20 mm × 0.15 mm) was made using thin spring steel (Tokushu Kinzoku Excel), and the flexible macrofiber composite (MFC, model: M8507-P2, Smart Material Corp.) sensor was used to measure the residual vibration of the flexible beam because it generates an output voltage on bending. The overall experimental setup of the SMA wire actuator is shown in figure 10(c): Two nitinol muscle wires (FLEXINOL® Actuator Wires, DYNALLOY, Inc.) with a diameter of 75 μm were used to make the series SMA wire actuator. A bias coil spring was installed to return to its initial position when the SMA wires were cooled, and an encoder

Table 2. Phase transformation temperatures of the SMA wires.

Parameter	SMA wire 1	SMA wire 2	SMA wire 3	SMA wire 4	SMA wire 5	SMA wire 6
A_s	68 °C	88 °C	52 °C	161 °C	64 °C	139 °C
A_f	78 °C	98 °C	62 °C	171 °C	74 °C	149 °C
M_s	52 °C	72 °C	36 °C	145 °C	48 °C	123 °C
M_f	42 °C	62 °C	26 °C	135 °C	38 °C	113 °C

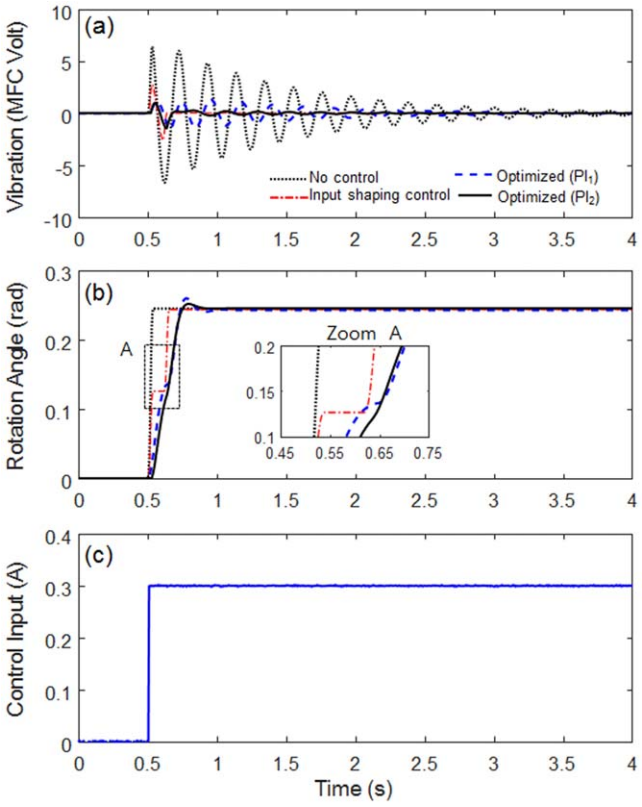

Figure 9. Simulation result for conventional actuator (motor) and series SMA wire actuator with optimized phase transformation temperatures (PI_1: 52 °C and 161 °C, PI_2: 64 °C and 139 °C): (a) residual vibration, (b) angular displacement of the pulley, and (c) control input of series SMA actuator (current).

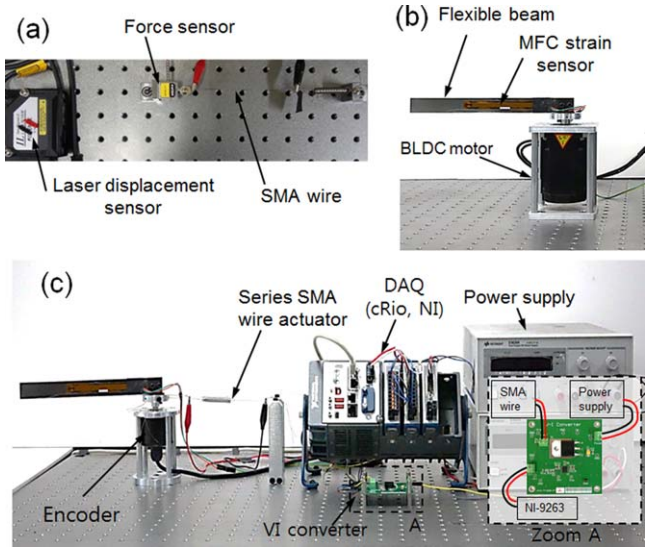

Figure 10. Photographs of the experimental setup for: (a) force hysteresis (b) input shaping control using conventional motor (ZV shaper), and (c) input shaping control using the series SMA wire actuator.

(E50S, Autonics) was installed to measure the rotation angle of the pulley. The commercially available SMA wire with phase transformations temperature of 68 °C (LT SMA wire) and 88 °C (HT SMA wire) were used for the series SMA wire actuator. A DC power of 12 V was supplied to a VI converter (HFA-002, Higgs), and an output voltage (0–5 V DC) from the NI-9263, analog voltage output module for cRio, was converted to 0–500 mA via the VI converter.

5.2. Results and discussion

Actuation force time responses of the series SMA wire actuator are presented in figure 11. We observed that while the rising time ranged from 0.48 s (LT SMA wire) to 0.69 s (HT SMA wire), the falling time ranged from 2.59 s (HT SMA wire) to 6.40 s (LT SMA wire), because the cooling is simply controlled by the convection in the surrounding air, which results in a much slower recovery response. This asymmetric property limits the SMA wire actuators to quasi-static applications such as input shaping control. While the stair-wise actuation force does not appear in the HT and LT SMA wires when the step current is applied, it appears in the series SMA wire, as shown in figure 11(a).

The proposed SMA wire actuator exhibits different actuation force hysteresis curves, as shown in figure 12. Because the experimental results of the actuation force hysteresis are in good agreement with the simulation results and the stair-wise actuation force is evidently observed in the series SMA wire, the concept of the series SMA wire actuator with different transformation temperatures has been successfully demonstrated.

As expected, the input shaping command can effectively suppress the residual vibration of the flexible beam manipulator, as shown in figure 13. By using the logarithmic decrement method [41], the natural frequency and damping ratio of the flexible beam was measured to be 4.57 Hz and 0.035, respectively, when the step input command was applied using the BLDC motor to design the stair-wise input shaping command (ZV shaper). Based on equation (15), the time locations (t_i) and amplitudes (A_i) of the ZV shaper were

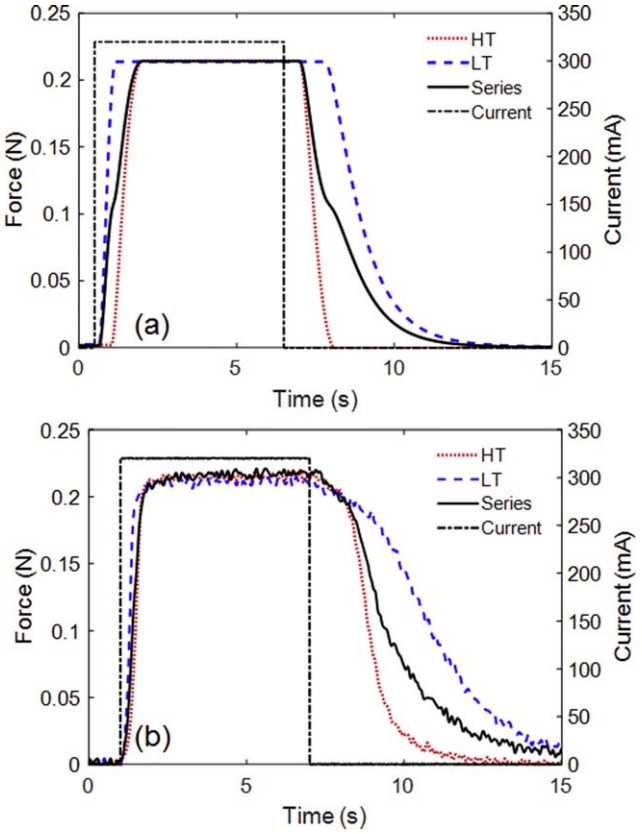

Figure 11. Actuation force time responses of series SMA wire actuator: (a) simulation, and (b) experiment.

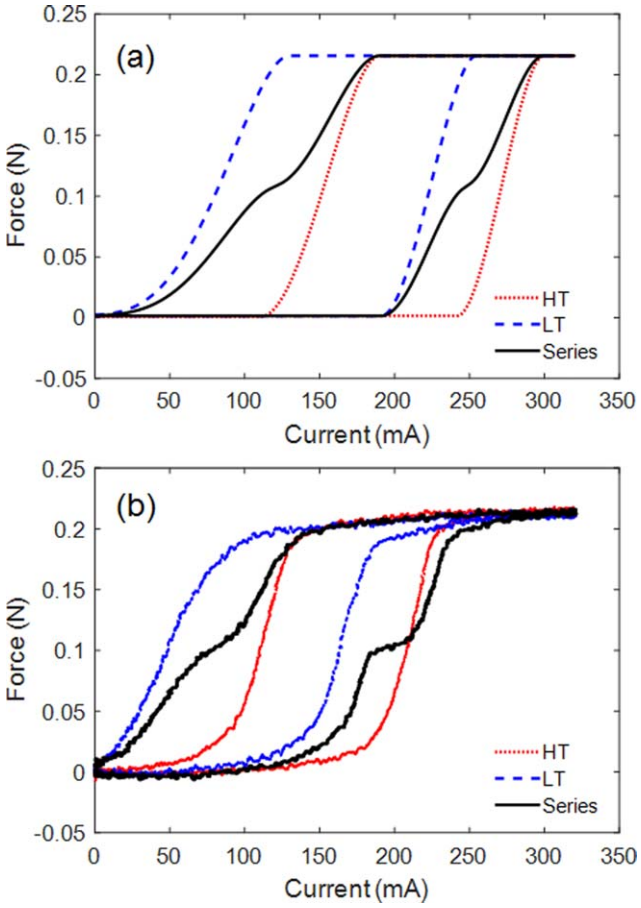

Figure 12. Actuation force hysteresis curves of the series SMA wire actuator: (a) simulation, and (b) experiment.

then determined as follows:

$$[t_i\ A_i] = \begin{bmatrix} 0 & 0.53 \\ 0.11 & 0.48 \end{bmatrix}. \tag{20}$$

To precisely track the desired input shaping command (i.e. the ZV shaper), the feedback motor controller was designed. A proportional gain (0.02) for a proportional controller (position loop), and a proportional gain (0.5), an integral gain (30) for a PI controller (velocity loop) was experimentally tuned so that the closed-loop system can possess stable poles.

The flexible beam manipulator actuated by a single (LT) SMA wire actuator exhibits a large residual vibration in response to the step control input, as shown in figure 14. This residual vibration becomes slightly alleviated when the proposed series SMA wire actuator consisting of different phase transformation temperatures (i.e. 68 °C and 88 °C) is used, as shown in figure 15. However, because the transformation temperature difference between the two SMA wires is not significant (or not optimized), there are limitations in implementing the ZV shaper. Therefore, to reproduce the ZV shaper as closely as possible, a different HT SMA wire ($\phi = 100\ \mu$m) was used. The time locations (t_i) and amplitudes (A_i) for input shaping control can then be estimated as follows:

$$[t_i\ A_i] = \begin{bmatrix} 0 & 0.58 \\ 0.19 & 0.42 \end{bmatrix}. \tag{21}$$

We observe that the residual vibration was incompletely suppressed; this is because the time location (i.e. $\Delta t = 0.19$ from equation (21)) does not match with the time location for the ZV shaper (i.e. $\Delta t = 0.11$ from equation (20)). Furthermore, from the simulation results (see figure 9), it is expected that this residual vibration can be further suppressed when the proposed series SMA wire actuator has optimum phase transformation temperatures (e.g. 52 °C and 161 °C, 64 °C and 139 °C), which is currently not available.

Thus, the proposed SMA actuator appears to offer potential applications in the new actuation system because of its many advantages over the conventional actuators (e.g. the electric motor) and single SMA actuators. The proposed series SMA wire actuator is simple but effective in suppressing residual vibration without sophisticated control input (see figure 13(c)), whereas an electric motor needs to be controlled using a complex electric driver and a motor controller such as closed-loop PID controller. Furthermore, the proposed SMA actuator does not require auxiliary circuitry, and the entire actuation system is lightweight (i.e. high power density). However, the manufacturing process of the SMA wire employing the desired phase transformation temperature

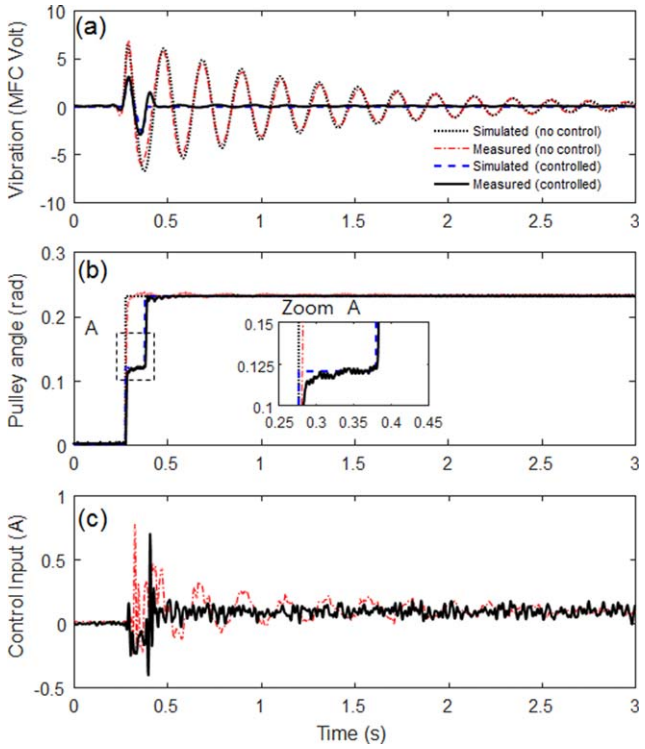

Figure 13. Results of input shaping control using the conventional actuator (BLDC motor): (a) residual vibration, (b) angular displacement of the pulley, and (c) motor control input.

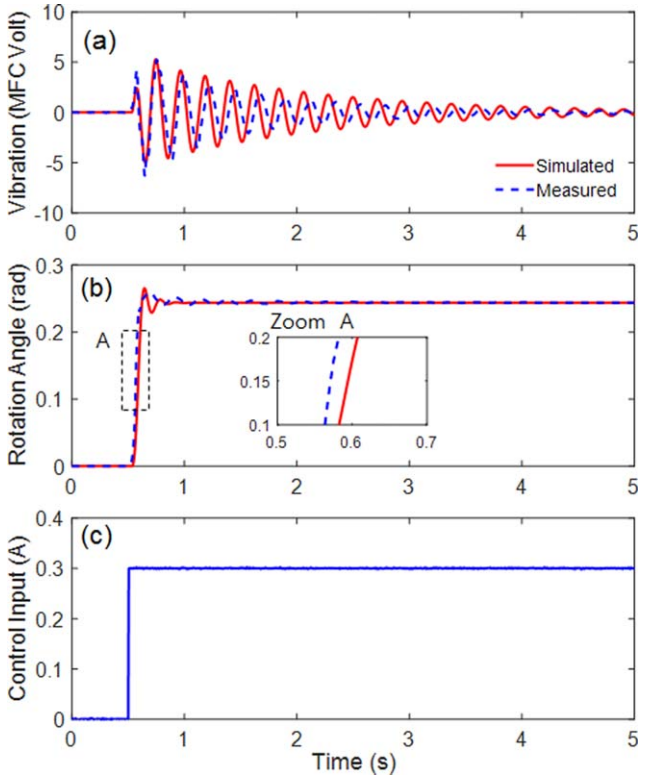

Figure 14. Comparison of simulation and experimental results of the single (LT) SMA wire actuator for a step control input: (a) residual vibration of the flexible beam, (b) angular displacement of the pulley, and (c) step input.

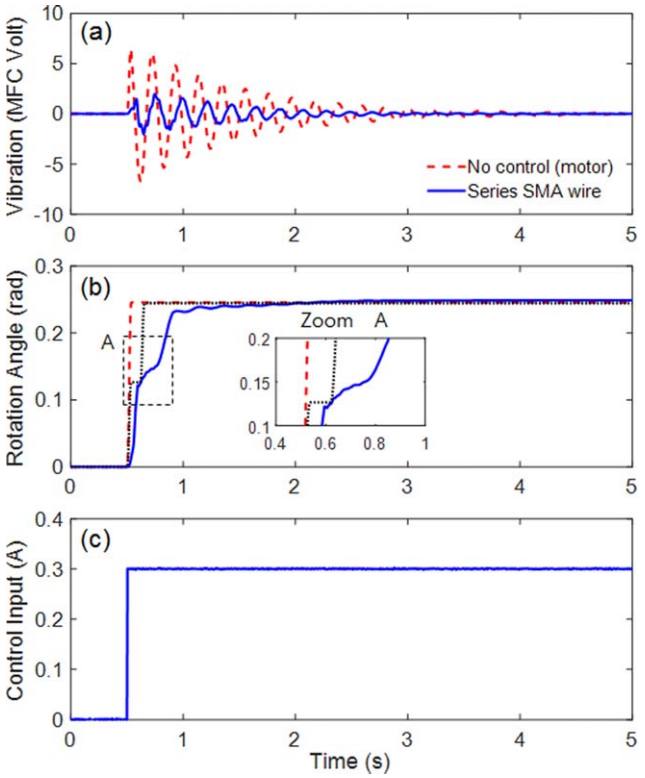

Figure 15. Comparison of the experimental results of the conventional actuator (BLDC motor) and series SMA wire actuator (LT, $\phi = 75$ μm and HT, $\phi = 100$ μm): (a) residual vibration of flexible beam, (b) angular displacement of the pulley (black dotted line; ZV shaper), and (c) step control input to series SMA wire actuator.

of SMA wires is challenging and expensive due to the difficulties involved in fine chemical composition tuning, which results in a few uncertainties. Additional potential uncertainties may also be induced by varying the mechanical properties of the SMA wire, depending on the phase transformation temperatures. However, these uncertainties can be compensated using a more robust input shaping control (i.e. a ZVD shaper). Therefore, further studies will be focused on overcoming the technical limitations of the proposed SMA wire actuator. For example, a series SMA wire actuator with optimum phase transformation temperatures enables complete suppression of the residual vibration, and therefore, its applications can be extended to multistep input shaping control.

6. Conclusion

A series SMA wire with different martensitic–austenitic phase transformation temperatures was successfully designed as a simple but efficient actuator for input shaping control of flexible structures (e.g. a beam manipulator). Its ability to suppress residual vibration was experimentally evaluated using a laboratory-level test-bed. The results demonstrated that the residual vibration of the flexible beam manipulator becomes slightly alleviated when the series SMA wire actuator consisting of different martensitic–austenitic phase

transformation temperatures (i.e. 154.4°F (68 °C) and 190.4° F (88 °C)) was employed. The proposed SMA actuator can effectively produce the stair-wise input shaping command by simply applying the step current input, which will be advantageous over the conventional actuators such as an electric motor in terms of efficiency and power density. Although this method of using series SMA wire actuator to produce input shaping effect offers promising applications for suppressing the residual vibration commonly present in actuating flexible deployable structures, there are technical problems that need to be further examined; for example, the manufacture of an SMA wire actuator consisting of optimum phase transformation temperatures is required to completely suppress the residual vibration.

Acknowledgments

This study was funded by INHA IST-NASA Deep Space Exploration Joint Research Center (NRF-2017K1A4A3013662).

ORCID iDs

Seung-Bok Choi https://orcid.org/0000-0001-6262-2815
Gi-Woo Kim https://orcid.org/0000-0003-4625-0382

References

[1] Macdonald M 2014 *Advances in Solar Sailing* (Chichester: Praxis)
[2] Wilkie W K, Warren J E, Horta L G, Lyle K H, Juang J, Littell J D, Bryant R G, Thomson M W, Walkemeyer P E and Guerrant D V 2014 Heliogyro solar sail research at NASA *Anonymous Advances in Solar Sailing* (Berlin: Springer) pp 631–50
[3] Harvey B, Smid H H and Pirard T 2010 Japan: into the solar system *Anonymous Emerging Space Powers* (Berlin: Springer) pp 37–99
[4] Fernandez J M, Schenk M, Prassinos G, Lappas V J and Erb S O 2013 Deployment mechanisms of a gossamer satellite deorbiter *ESMATS 2013*
[5] Nishiyama Y 2012 Miura folding: applying origami to space exploration *Int. J. Pure Appl. Math.* **79** 269–79
[6] Fernandez J M, Viquerat A, Lappas V J and Daton-Lovett A J 2014 Bistable over the whole length (BOWL) CFRP booms for solar sails *Anonymous Advances in Solar Sailing* (Berlin: Springer) pp 609–28
[7] Dowell E H 2011 Can solar sails flutter? *AIAA J.* **49** 1305–7
[8] Shan J, Liu H and Sun D 2005 Modified input shaping for a rotating single-link flexible manipulator *J. Sound Vib.* **285** 187–207
[9] Subudhi B and Morris A S 2002 Dynamic modelling, simulation and control of a manipulator with flexible links and joints *Robot. Auton. Syst.* **41** 257–70
[10] Kojima H and Singhose W 2007 Adaptive deflection-limiting control for slewing flexible space structures *J. Guid. Control Dyn.* **30** 61–7
[11] Turner J D and Chun H M 1984 Optimal distributed control of a flexible spacecraft during a large-angle maneuver *J. Guid. Control Dyn.* **7** 257–64
[12] Singhose W 2009 Command shaping for flexible systems: a review of the first 50 years *Int. J. Precis. Eng. Manuf.* **10** 153–68
[13] Song G, Buck N V and Agrawal B N 1999 Spacecraft vibration reduction using pulse-width pulse-frequency modulated input shaper *J. Guid. Control Dyn.* **22** 433–40
[14] Hu Q and Ma G 2005 Variable structure control and active vibration suppression of flexible spacecraft during attitude maneuver *Aerosp. Sci. Technol.* **9** 307–17
[15] Smith O J 1957 Posicast control of damped oscillatory systems *Proc. IRE* **45** 1249–55
[16] Bailey T and Hubbard J E 1985 Distributed piezoelectric-polymer active vibration control of a cantilever beam *J. Guid. Control Dyn.* **8** 605–11
[17] Han J and Lee I 1999 Optimal placement of piezoelectric sensors and actuators for vibration control of a composite plate using genetic algorithms *Smart Mater. Struct.* **8** 257
[18] Choi S, Hong S, Sung K and Sohn J 2008 Optimal control of structural vibrations using a mixed-mode magnetorheological fluid mount *Int. J. Mech. Sci.* **50** 559–68
[19] Lara-Prieto V, Parkin R, Jackson M, Silberschmidt V and Kęsy Z 2009 Vibration characteristics of MR cantilever sandwich beams: experimental study *Smart Mater. Struct.* **19** 015005
[20] Otsuka K and Wayman C M 1999 *Shape Memory Materials* (Cambridge: Cambridge University Press)
[21] Sun L, Huang W M, Ding Z, Zhao Y, Wang C C, Purnawali H and Tang C 2012 Stimulus-responsive shape memory materials: a review *Mater Des.* **33** 577–640
[22] Baz A, Imam K and McCoy J 1990 Active vibration control of flexible beams using shape memory actuators *J. Sound Vib.* **140** 437–56
[23] Sohn J W, Han Y M, Choi S B, Lee Y S and Han M S 2009 Vibration and position tracking control of a flexible beam using SMA wire actuators *J. Vib. Control.* **15** 263–81
[24] Jani J M, Leary M, Subic A and Gibson M A 2014 A review of shape memory alloy research, applications and opportunities *Mater. Des.* **56** 1078–113
[25] Flemming L and Mascaro S 2012 Analysis of hybrid electric/thermofluidic inputs for wet shape memory alloy actuators *Smart Mater. Struct.* **22** 014015
[26] Zhang X, Hu J, Mao S, Dong E and Yang J 2014 Design and property analysis of a hybrid linear actuator based on shape memory alloy *Smart Mater. Struct.* **23** 125004
[27] Leng J, Yan X, Zhang X, Huang D and Gao Z 2016 Design of a novel flexible shape memory alloy actuator with multilayer tubular structure for easy integration into a confined space *Smart Mater. Struct.* **25** 025007
[28] Shim J, Quan Y, Wang W, Rodrigue H, Song S and Ahn S 2015 A smart soft actuator using a single shape memory alloy for twisting actuation *Smart Mater. Struct.* **24** 125033
[29] Sheng J and Desai J P 2015 Design, modeling and characterization of a novel meso-scale SMA-actuated torsion actuator *Smart Mater. Struct.* **24** 105005
[30] Rodrigue H, Wei W, Bhandari B and Ahn S 2015 Fabrication of wrist-like SMA-based actuator by double smart soft composite casting *Smart Mater. Struct.* **24** 125003
[31] Paik J K, Hawkes E and Wood R J 2010 A novel low-profile shape memory alloy torsional actuator *Smart Mater. Struct.* **19** 125014
[32] Paik J K and Wood R J 2012 A bidirectional shape memory alloy folding actuator *Smart Mater. Struct.* **21** 065013
[33] Sohn J, Kim G and Choi S 2018 A state-of-the-art review on robots and medical devices using smart fluids and shape memory alloys *Appl. Sci.* **8** 1928

[34] Technical Characteristics of Flexinol® Actuator Wires, Dynalloy Inc, Irvine, CA
[35] Mihálcz I 2001 Fundamental characteristics and design method for nickel–titanium shape memory alloy *Period. Polytech. Mech. Eng.* **45** 75–86
[36] Liang C and Rogers C A 1997 One-dimensional thermomechanical constitutive relations for shape memory materials *J. Intell. Mater Syst. Struct.* **8** 285–302
[37] Choi S, Cheong C and Shin H 1995 Sliding mode control of vibration in a single-link flexible arm with parameter variations *J. Sound Vib.* **179** 737–48
[38] MATLAB/Simulink™ V7.6, *2011 User's guide*, The Mathworks
[39] Houck C R, Joines J and Kay M G 1995 A genetic algorithm for function optimization: a Matlab implementation *Ncsu-ie tr.* **95** 1–10
[40] Passino K M 2005 *Biomimicry for Optimization, Control, and Automation* (London: Springer Science & Business Media)
[41] de Silva C W 2007 *Vibration Damping, Control, and Design* (Boca Raton, FL: CRC Press)